Accelerated ultrafast demagnetization of an interlayer-exchange-coupled Co/Mn/Co trilayer

Jendrik Gördes o, ¹ Ivar Kumberg o, ¹ Chowdhury S. Awsaf o, ¹ Marcel Walter o, ¹ Tauqir Shinwari o, ¹ Sangeeta Thakur o, ¹ Sangeeta Sharma, 1,2 Christian Schüßler-Langeheine, 3 Niko Pontius, 3 and Wolfgang Kuch. ¹Institut für Experimentalphysik, Freie Universität Berlin, Arnimallee 14, 14195 Berlin, Germany ²Max-Born-Institut für Nichtlineare Optik und Kurzzeitspektroskopie, Max-Born Straße 2a, 12489 Berlin, Germany ³Helmholtz-Zentrum Berlin für Materialien und Energie, Albert-Einstein-Straße 15, 12489 Berlin, Germany

(Received 30 May 2025; revised 8 August 2025; accepted 9 September 2025; published 26 September 2025)

We investigate the ultrafast magnetization dynamics of an interlayer-exchange-coupled Co/Mn/Co trilayer system after excitation with an ultrafast optical pump. We probe element- and time-resolved ferromagnetic order by x-ray magnetic circular dichroism in resonant reflectivity. We observe an accelerated Co demagnetization time in the case of weak total parallel interlayer coupling at 9.5 ML Mn thickness for antiparallel alignment of both Co layers compared to parallel alignment as well as for parallel alignment in the case of strong parallel interlayer coupling at 11 ML of Mn. From ab initio time-dependent density functional theory calculations, we conclude that optically induced intersite spin transfer of spin-polarized electrons from Co into Mn acts as a decay channel to enhance and accelerate ultrafast demagnetization. This spin transfer can only take place in case of a collinear Mn spin structure. We argue that this is the case for antiparallel alignment of both Co layers at 9.5 ML Mn thickness and parallel alignment in case of 11 ML of Mn. Our results point out that an antiferromagnetic spacer layer and its spin structure have a significant effect on the magnetization dynamics of adjacent ferromagnetic layers. Our findings provide further insight into fundamental mechanisms of ultrafast demagnetization and may lead to improve dynamics in multilayered systems for faster optical switching of magnetic order.

DOI: 10.1103/h2cw-hdvm

I. INTRODUCTION

Driving spin dynamics of magnetic thin films by ultrashort laser pulses provides the opportunity to manipulate the magnetic order on the femtosecond timescale and has gathered interest since pioneering experiments by Beaurepaire et al. on Ni in 1996 [1-6]. A number of different theoretical approaches have been employed to explain ultrafast magnetization dynamics, e.g., via superdiffusive spin currents [7–12], magnons [13,14], or (Elliott-Yafet, electron-electron, electron-phonon) spin-flip scattering [15–17].

Recently, a laser-induced spin-selective excitation of electrons between magnetic sublattices, so-called optically induced intersite spin transfer (OISTR) [18], has emerged as a mechanism to enable extremely fast all-optical manipulation of magnetic order. Because of its purely optical nature, spin dynamics can be induced on timescales shorter than the exchange interaction. Since its theoretical prediction, numerous experiments have confirmed the presence of OISTR, starting by using time-resolved magnetic circular dichroism to observe a faster demagnetization of ferromagnetic (FM) Ni in Ni/Pt multilayers compared to a pure Ni layer [19]. Later, studies revealed the effect of intersite spin transfer on

Published by the American Physical Society under the terms of the Creative Commons Attribution 4.0 International license. Further distribution of this work must maintain attribution to the author(s) and the published article's title, journal citation, and DOI.

the enhanced demagnetization of a CoPt alloy in comparison to pure Co [20], as well as a transient FM state of antiferromagnetic (AFM) Mn in Co/Mn multilayers [21]. Using transverse magneto-optical Kerr effect in the extreme ultraviolet region, the OISTR effect could be verified in an FeNi alloy and Heusler half-metal [22,23]. Very recently, time- and angle-resolved photoemission spectroscopy revealed OISTR to induce a spin-selective charge flow between surface and bulk states in metallic Gd during laser-driven demagnetization, causing a transient increase of the bulk-band exchange splitting [24].

The interface plays an important role for the magnetization dynamics of a FM layer as the FM can be influenced either by direct or indirect interlayer exchange coupling. Kumberg et al. [12] observed an accelerated demagnetization of a FM Ni or Co layer in the presence of antiferromagnetic order in an adjacent NiMn layer, which was attributed to superdiffusive spin currents between the AFM and the FM layer. In the case of a Ni/Ru/Fe FM/spacer/FM trilayer system [10], where the magnetization of both FM layers can either be parallel or antiparallel to each other, a transiently enhanced magnetization (parallel) or reduced magnetization (antiparallel) of Fe was observed after an optical pump pulse and attributed to superdiffusive spin currents. Interestingly, a faster demagnetization of Ni was measured in the case of antiparallel alignment but not discussed further. A faster and larger amount of demagnetization for antiparallel alignment of two out-of-plane magnetized FM layers was also observed in the [CoPt]_n/Ru/[CoPt]_n [7] multilayer system. It was argued that a direct transfer of spin angular momentum between both CoPt layers takes place via superdiffusive spin currents, which

^{*}Contact author: kuch@physik.fu-berlin.de

can travel through the metallic Ru spacer but are blocked by insulating AFM NiO.

In this article, we report on the influence of an AFM Mn spacer layer on the magnetization dynamics of adjacent FM Co layers after excitation by an ultrashort laser pulse. For the epitaxial Co/Mn/Co thin-film system, a combination of direct exchange coupling through the spin structure of the AFM layer, orange-peel coupling, and Ruderman-Kittel-Kasuya-Yosida (RKKY)-type coupling results in a Mn-thickness-dependent oscillatory interlayer coupling energy between the two Co layers across the Mn layer [25]. By growing the Mn layer as a wedge, different coupling regimes are accessible. We use resonant soft-x-ray magnetic circular dichroism in reflectivity (R-XMCD) to probe the magnetization dynamics after excitation with an ultrashort infrared pulse with elemental and time resolution. Remarkably, we observe an accelerated demagnetization not only in the case of initial antiparallel alignment of both Co layers, in agreement with results from [7] and [10], but also for parallel alignment in the case of a Mn thickness leading to strong parallel interlayer coupling. Applying ab initio time-dependent density functional theory (TD-DFT) calculations, we identify this behavior to originate from the OISTR effect as the dominant mechanism because of an additional decay channel from a spin-selective transfer of spin-polarized electrons from Co into Mn. Depending on the alignment of both FM layers with respect to the sign of the interlayer coupling by direct exchange through the Mn layer, the Mn spin structure is either collinear or twisted, resulting in OISTR or less OISTR, respectively.

II. EXPERIMENT

The sample consists of Cu(001)/8 ML Co/7-11 ML Mn(wedge)/20 ML Co/6 ML Ni and was grown under ultrahigh vacuum conditions via molecular beam epitaxy. Before evaporation, the Cu(001) single crystal was cleaned by Ar⁺ sputtering and annealed at a temperature of 850 K for 30 min. Substrate cleanliness was checked by Auger electron spectroscopy (AES) and low-energy electron diffraction (LEED). The base pressure of the UHV chamber was around 5×10^{-10} mbar, while the pressure during layer deposition was kept in the lower 10^{-9} mbar region. During evaporation, a quartz crystal microbalance (QCM) and oscillations from medium-energy electron diffraction (MEED) were used to monitor and ensure layer-by-layer growth of the Co bottom layer and the first 7 ML of Mn. For the last 4 ML of Mn, a shutter was placed in front of the moving substrate to grow Mn in a wedge. Deposition of Co and Ni top layers was monitored by QCM since there are no MEED oscillations observable for deposition on the Mn wedge. The layer thickness was additionally checked via AES after deposition of each layer. Magnetic properties of the sample were measured with longitudinal magneto-optical Kerr effect (L-MOKE) at different positions along the wedge. Previous experiments [25] had shown a Mn-thickness-dependent oscillatory interlayer coupling energy between the two ferromagnetic Co layers across the antiferromagnetic Mn layer. Depending on the Mn thickness, either a ferromagnetic coupling or an antiferromagnetic coupling between both Co layers was observed. The reason

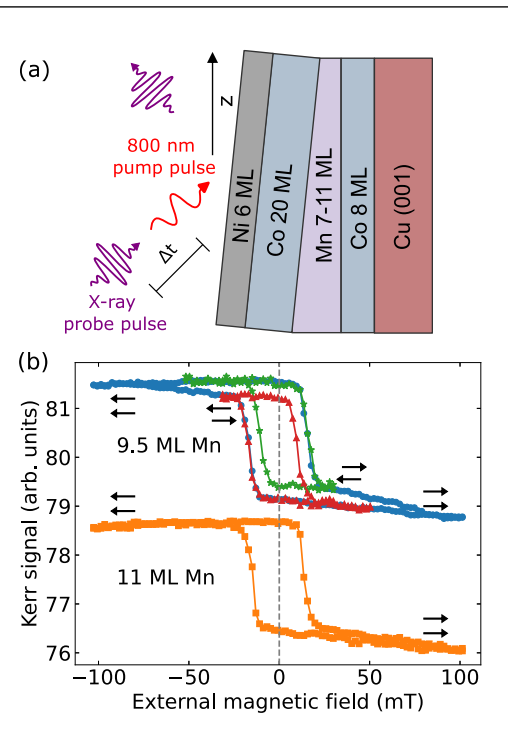


FIG. 1. (a) Sketch of the experiment. Sample geometry of the Cu(001)/Co/Mn/Co/Ni layer system. (b) The hysteresis loop in the SC regime (orange) shows a one-step magnetization reversal (indicated by black arrows), while in the weak coupling regime (blue) first the top Co layer switches and then the bottom Co layer. Minor loops taken after positive (red) and negative saturation (green) in the WC regime exhibit a positive horizontal shift indicating parallel interlayer coupling.

for this oscillatory behavior was concluded to be from the combination of direct exchange interaction as well as RKKY interaction [26], with different periods of oscillation: While the oscillation period of the direct exchange interaction is 2 ML, about 5–6 ML period is expected from the RKKY interaction [25]. In addition, the constant, non-oscillatory magnetostatic interlayer coupling owing to correlated interface roughnesses [27,28] adds a parallel coupling energy.

We performed time-resolved experiments at two different Mn thicknesses, corresponding to two different coupling regimes: a strong and a weak parallel coupling regime [Fig. 1(b)]. In the weak coupling (WC) regime at a Mn thickness of about 9.5 ML, magnetization reversal proceeds via a two-step process, one relatively sharp at about 15 mT and a broader and smaller one at around 60 mT. L-MOKE measurements for different Co top-layer thicknesses of 5 ML, 10 ML, and 15 ML reveal a reduction of the coercivity of only the first step with the top Co layer thickness, showing that with increasing field first the top Co (and Ni) layer and then the bottom Co layer reverse magnetization. In the strong coupling (SC) regime at a Mn thickness of about 11 ML, there is a single step in the hysteresis loop because both Co layers reverse their magnetization direction together. Another WC regime is observed at a Mn thickness of about 8 ML. Minor loops [Fig. 1(b)] in the WC regime show a horizontal shift of about 3.5 mT in the direction of the magnetic field opposite to the saturation for the reversal of the top Co layer, indicating a parallel interlayer coupling. No antiferromagnetic coupling

could be observed in the thickness range of 7-11 ML. In the SC regime, a determination of the coupling strength via the shift of minor loops is not possible since there is only a single magnetization reversal step. This behavior is consistent with the results from Ref. [25], where the coupling energy between two Co films across a Mn film has been measured for Mn thicknesses from 11 to 17 ML. Maxima of antiparallel coupling of the direct exchange coupling have been observed at 11.5, 13.5, and 15.5 ML Mn, while an antiparallel coupling maximum of the RKKY coupling was located at 13.7 ML. Considering the systematic uncertainty of the thickness determination of the Mn wedge of about 10%, we conclude that at 9.5 ML we are close to an antiparallel maximum of the direct exchange and a parallel maximum of the RKKY coupling. Together with the magnetostatic interaction favoring parallel alignment, the overall coupling is weakly parallel. At 11 ML, both the direct exchange and the RKKY coupling favor parallel alignment of the Co layers, leading to the observed strong parallel coupling. In this case, the magnetizations of both Co layers switch simultaneously if their coercivity is smaller than the coupling field. We think that the different magnetization reversal characteristics and the different coercive fields of the two Co layers are, on the one hand, because of the different thicknesses of the two layers, since interface-related contributions to the coercivity scale inversely proportional to the FM-layer thickness. Other contributing factors could be growth-related differences in interface and structural quality of the two layers, resulting in a stronger FM-AFM coupling at the lower interface, or somewhat different magnetic anisotropies of the two FM layers.

The sample was transferred to the FemtoSlicing Facility at BESSY II [29] within a vacuum suitcase without breaking UHV. There, time-resolved scattering experiments were carried out with a 100 fs full-width half-maximum (FWHM) circularly polarized soft-x-ray probe pulse and a 60 fs FWHM 800 nm p-polarized pump pulse from a Ti:Sa laser amplifier system. Both pulses are intrinsically synchronized and propagate close to collinear. The size of the pump laser spot on the sample was $(1500 \times 200) \,\mu\text{m}^2$ while the size of the x-ray probe pulse was $(140 \times 40) \, \mu \text{m}^2$. The slicing setup runs with a 6 kHz repetition rate that is split to record the unpumped and pumped signal in an alternating order for each data point. We optimized the angle of incidence and the photon energy to get the best combination of signal strength and magnetic contrast [30]. This was the case at the Co L_3 edge for an angle of incidence of 7° and an energy of 780.4 eV.

An external magnetic field was applied along the x-ray incidence direction, close to in-plane to the sample, to reverse the magnetic order of the FM layers at each data point in order to record the R-XMCD. Different thicknesses of the Mn wedge were reached by translation of the sample in the vertical direction. R-XMCD hysteresis loops at the Co L_3 edge show a one- or two-step reversal in dependence on the Mn thickness, in agreement with our L-MOKE measurements (Fig. S3 within the Supplemental Material [31]).

A magnetic field of 150 mT was used for parallel (WCP) alignment of bottom and top Co layers, while a sequence of 150 mT and a reverse field of 25 mT was used to set an antiparallel (WCA) alignment in the case of weak coupling at 9.5 ML Mn thickness. In the case of strong coupling at 11 ML

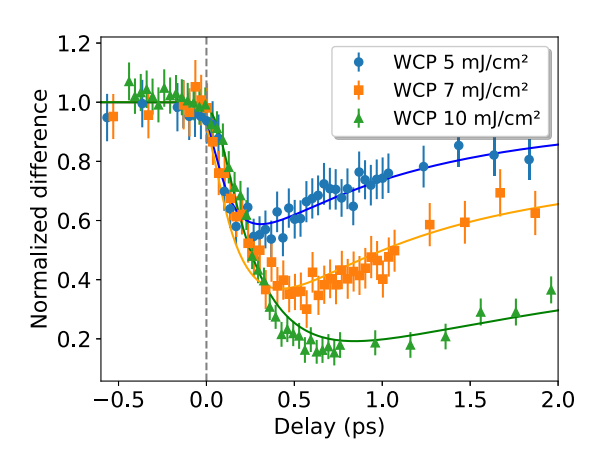


FIG. 2. Pump-probe delay time traces of the normalized difference for parallel orientation of the Co magnetizations at 9.5 ML Mn thickness at different laser fluences. Continuous lines represent exponential fits as described in the text.

Mn thickness, the magnetization of both Co layers could only be oriented in parallel (SCP). A pump fluence range of 5–10 mJ/cm² peak fluence was chosen to vary the range from full demagnetization to considerable demagnetization while still avoiding nonreversible effects like photo-bleaching over the time of the measurements.

III. RESULTS

We measured the reflected soft-x-ray signal at the Co L_3 edge as a function of pump-probe delay time to study the influence of the AFM spacer layer on the ultrafast magnetization dynamics of the coupled Co layers. For each step of the delay time, pumped and unpumped intensity were recorded for opposite magnetizations of the Co layers M^+ and M^- , resulting in a total of four signals. The scans were normalized by dividing the difference $(M^+ - M^-)$ of the pumped signals by the difference of the unpumped signals, which we define as the normalized difference. Error bars were calculated using error propagation and the total photon count N, so that the error scales with \sqrt{N} . Calculations of the layerwise optical differential absorption at 800 nm wavelength, according to [32,33], show an absorption of 16.5% for the top Co layer and 4.8% for the bottom Co layer (Fig. S6 within the Supplemental Material [31]). Since the top Co layer is 2.5 times as thick as the bottom Co layer, Co atoms in the top layer absorb on average only about 35% more pump intensity than the ones in the bottom layer. Magnetic moments in both layers are thus pumped not too differently by the pump pulse and hot electrons will be excited in both layers.

Pump-probe delay scans are shown in Fig. 2 for incident pump laser fluences of 5, 7, and 10 mJ/cm², taken at room temperature with an external field of $\pm 150\,\mathrm{mT}$ to saturate the sample and align both Co layers in parallel. The normalized difference reaches a minimum within 600 fs for all three fluences, although a shorter demagnetization time is required for smaller fluences (similar to results from [12] and [16]). The demagnetization amplitude increases with increasing fluence, resulting in a nearly complete demagnetization at a fluence of $10\,\mathrm{mJ/cm^2}$. Remagnetization, indicated by an increase of

normalized difference with delay time, takes longer for larger pump fluences as more energy needs to be dissipated to return to equilibrium, and is in agreement with previous observations [34].

To evaluate the magnetization dynamics quantitatively, we fitted our measurements to the sum of three exponential functions. One exponential describes the ultrafast demagnetization and the other two a fast initial and a slower subsequent remagnetization. Additionally, the sum is convoluted by a Gaussian g(t) with a FWHM of 120 fs to consider the temporal resolution of the experiment. This results in the following equation:

$$\frac{M}{M_0}(t) = g(t) \otimes \left[\Theta(t - t_0) \left(a \left(e^{-(t - t_0)/t_m} - 1 \right) - b \left(e^{-(t - t_0)/t_f} - 1 \right) - c \left(e^{-(t - t_0)/t_s} - 1 \right) \right) + C \right],$$
(1)

where Θ is the Heaviside step function, t_m , t_f , and t_s the time constants for demagnetization and fast and slow remagnetization, and a, b, and c are the corresponding de- and remagnetization amplitudes, respectively. C is an offset to start the fitting function before time zero at the same value as the normalized measurement data. Time t_0 is a shift to accommodate for slow drifts in pump-probe delay time between measurements to have a common time zero for all fluences. For the present data, a slow continuous drift of about 900 fs in t_0 was present over the course of the nine data sets taken, which were measured in about 96 hours. We can thus not exclude drifts of the order of 100 fs within a single data set. [Overall, for long time windows (~100 ps), remagnetization amplitudes b and c should be equal to the demagnetization amplitude a, which was not enforced but usually the case during fitting.] The resulting fit curves for all the experimental data and the corresponding fit parameters can be found in the Supplemental Material [31].

We study the influence of the AFM spacer layer by recording pump-probe delay scans at the two different selected Mn thicknesses to compare the dynamics when both Co layers are weakly and strongly coupled (SCP). Additionally, in the case of weak coupling at 9.5 ML of Mn, we looked at ultrafast magnetization dynamics in the case of antiparallel (WCA) and parallel (WCP) alignment of top and bottom Co layers. In the WCP case, Mn spins need to twist within the AFM spacer layer to accommodate both Co layers, since the direct exchange coupling between Mn and Co favors an antiparallel alignment.

Delay scans and fit results are presented in Fig. 3 for all three cases for a pump fluence of $10\,\mathrm{mJ/cm^2}$. Extracted time constants for pump fluences of 5, 7, and $10\,\mathrm{mJ/cm^2}$ are listed in Table I. Comparing WCP and WCA (Fig. 3 blue and cyan), we measure a significantly faster demagnetization of $90\pm20\,\mathrm{fs}$ in the antiparallel case compared to $240\pm40\,\mathrm{fs}$ in the parallel case for a fluence of $10\,\mathrm{mJ/cm^2}$.

In the case of SCP (Fig. 3 red) at 11 ML of Mn, where only parallel alignment of both Co layers is achievable, a fast demagnetization of 78 ± 14 fs was measured, with a value in the range of the WCA case. This is quite surprising, as one would assume a slower demagnetization for parallel alignment in the case of superdiffusive spin currents, which thus cannot explain this behavior and will be discussed in the following.

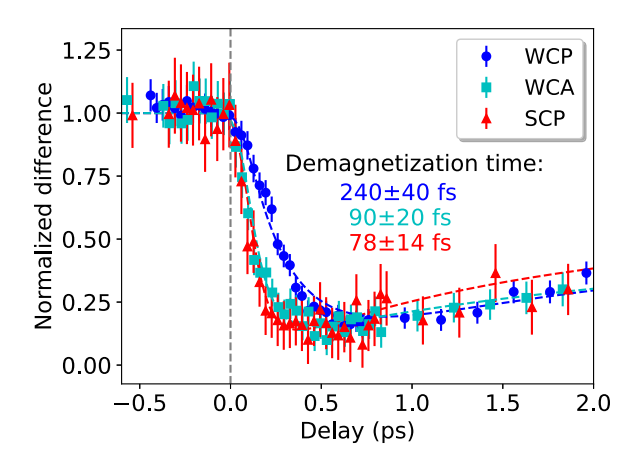


FIG. 3. Pump-probe delay time traces for a fluence of 10 mJ/cm² for WCP (blue), WCA (cyan), and SCP (red). The dashed lines are the corresponding fit functions.

IV. DISCUSSION

Since the accelerated ultrafast demagnetization of the Co layers takes place within the first 100–200 fs after pumping the system, faster than the typical timescale for equilibration with the lattice, the effect seems to be electronic in nature. As mentioned before, the exchange of spin currents between the two FM layers would explain the different demagnetization times for parallel and antiparallel alignment of the FM layers in the WCP and WCA case, but cannot explain the observed accelerated demagnetization in the SCP case. We thus attribute the difference in demagnetization times to the spin structure of the AFM Mn spacer layer. Based on a comparison with our previous static experiments on Co/Mn/Co/Cu(001) [25], as argued in Sec. II, we assume that in the case of WCA and WCP, the direct exchange coupling across the Mn layer favors antiparallel alignment of the adjacent Co layers. Thus, there is a low-energy collinear Mn spin structure in the case of antiparallel alignment of both Co layers, while for parallel alignment, Mn spins need to twist within the layer to accommodate both Co layers to which they couple

TABLE I. Demagnetization time constant t_m as well as fast t_f and slow t_s remagnetization time constants in dependence of pump laser fluence in case of parallel (WCP, SCP) or antiparallel (WCA) alignment of both Co layers. For SC, only parallel alignment (SCP) is possible because of strong interlayer coupling. The errors are the uncertainties from the fits alone.

Fluence	Alignment	t_m [ps]	t_f [ps]	t_s [ps]
5 mJ/cm ²	WCP WCA SCP	0.12 ± 0.02 0.11 ± 0.04 0.11 ± 0.04	1.0 ± 0.2 0.5 ± 0.3 0.5 ± 0.2	$ 19 \pm 11 \\ 5 \pm 3 \\ 6 \pm 4 $
7 mJ/cm ²	WCP WCA SCP	0.17 ± 0.05 0.10 ± 0.03 0.08 ± 0.02	0.8 ± 0.3 0.7 ± 0.2 1.1 ± 0.3	8 ± 2 13 ± 3 17 ± 7
10 mJ/cm^2	WCP WCA SCP	0.24 ± 0.04 0.09 ± 0.02 0.08 ± 0.01	2.0 ± 0.5 2.1 ± 0.5 1.6 ± 0.3	110 ± 40 210 ± 160 60 ± 20

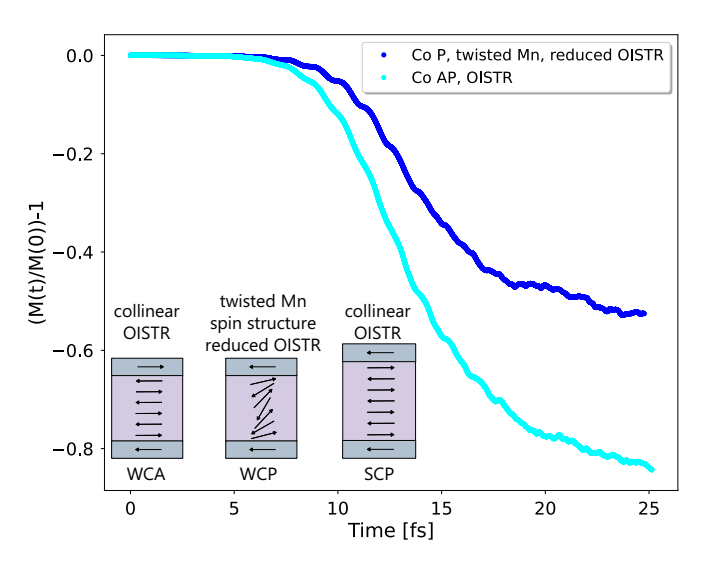


FIG. 4. Result of a TD-DFT calculation of the time-dependent magnetic moment of Co for a Co-Co-Mn-Mn-Mn-Mn-Co-Co layer system after excitation with a 12.4 fs FWHM 800 nm laser pulse with a fluence of 29 mJ/cm² in the case of antiparallel (cyan) and parallel (blue) alignment of Co spins on opposite sides of the trilayer. The graph shows the change in the sum of the absolute value of the magnetic moments of the Co layers on both sides of the Mn spacer layer. The differences in demagnetization dynamics and amplitude of the Co layers for parallel and antiparallel alignment appear as a result of OISTR with the sandwiched Mn layer. (Inset) Schematic of Mn spin structure for the WCP, WCA and SCP case. Direct coupling of Mn spins with Co spins causes Mn spins within the layer to twist in the case of WCP, such that OISTR is reduced between Co and Mn atoms (the twisting is sketched here as perpendicular to the film plane, but could as well be in the film plane).

directly at the interface, increasing the exchange energy. For a Mn thickness of 9.5 ML, the twist angle between adjacent atomic planes can be estimated to be of the order of 20°, but, because of interface roughness, is probably more than that at the upper interface between Mn and Co. In the case of SCP, the direct exchange favors parallel alignment, such that the AFM spin structure rests in a collinear configuration. This is schematically depicted in the inset of Fig. 4. Figure 3 and Table I thus show a clear dependence of the time constant of the ultrafast optical demagnetization of the Co layers on the Mn spin structure. Because of the ultrafast nature of the effect, we attribute this observation to the OISTR effect.

To support this assumption and to explore this phenomenon qualitatively, we use TD-DFT, based on a fully noncollinear version of the Elk code [35,36]. We model the system by a stack of 2 ML Co, 4 ML Mn, and 2 ML Co. Since OISTR is an effect that is most prominent between nearest neighbors, extra layers are not needed to unravel the necessary physics [18]. We calculate the dynamic optical response after excitation with a pump pulse of 29 mJ/cm² fluence with a wavelength of 800 nm and a FWHM of 12.4 fs, which is shorter than the employed 60 fs pump pulse, but should show the same effects, as shown in [19]. Figure 4 shows the time-dependent relative change of the sum of the absolute values of the magnetic moments of both Co layers after excitation with a pump pulse for alignment of the Co magnetizations in parallel (P, blue)

and antiparallel (AP, cyan). The calculations clearly show that there is indeed a large difference in dynamics between parallel and antiparallel alignment of both Co layers coming from OISTR between Co and Mn atoms. For the idealized system considered in the calculations, the even number of Mn atomic monolayers means a collinear spin structure for antiparallel Co magnetizations and a twisted one for parallel. The OISTR mechanism is strongly governed by the number of available states, which is large (maximum possible) for a fully AFM configuration between Co and Mn. In a twisted noncollinear spin configuration this number of available states, projected in the direction of Co spins, automatically reduces, reducing the OISTR effect.

From the TD-DFT calculations, we can see that the OISTR effect is strongest for AFM alignment of spins at the Co–Mn interfaces and, to a lesser extent, also of spins between Mn atoms. Noncollinear alignment of spins (i.e., canting angle between spins away from antiparallel alignment) reduces the OISTR effect and it becomes minimal for the limiting case of parallel alignment. The reason for this has been identified to the fact that for the antiparallel case the optically excited electrons have a maximum number of available states allowing for large OISTR effect [37,38]. From this we can see that when the spin slowly cants away from perfect alignment in the case of several layers of Mn, the OISTR effect is more and more suppressed.

This can be transferred to explain our experimental results, as shown in the inset of Fig. 4: the presence of OISTR in the WCA case and in the SCP case result in an accelerated ultrafast demagnetization of the Co layers. For WCP, the direct exchange coupling through the Mn layer leads to a twisted Mn spin structure. As a result, there is less OISTR in the latter configuration. The mechanism in OISTR is that unoccupied minority states in Mn can act as a spin sink for majority spins from Co. The demagnetization time decreases as a result of optical transfer of spin-polarized electrons from both Co layers into Mn, which acts as a decay channel. Both, the calculations and the experiments confirm that the spin structure of the AFM spacer layer influences significantly the magnetization dynamics of adjacent FM layers after an ultrafast optical excitation. While the experimentally observed demagnetization amplitudes are about the same for the collinear and the twisted Mn spin structure, the calculations show different amplitudes at 25 fs. We speculate that effects not covered within the time span of the TD-DFT calculation could lead to the experimentally observed equal demagnetization amplitude in the two cases.

We note that spin-dependent interface transmittance of hot electrons from the Co layers into the sandwiched Mn layer, assuming a reduced spin penetration depth in the case of twisted Mn spin structure, could be another explanation. In [7] and [10], an accelerated demagnetization in the antiparallel case has been observed and explained via superdiffusive spin currents. However, in both cases only a relatively low pump fluence (0.65 mJ/cm² and 2 mJ/cm², respectively) was used to avoid competing processes, because at high pump fluences superdiffusive spin currents become saturated or even less effective close to full demagnetization [8,10,39]. In our case, larger pump fluences were used, at which the OISTR effect becomes relevant and the effect of superdiffusive spin currents

negligible. Differences in interface quality between the top Co layer and Mn could, in principle, also change the magnetization dynamics between thin (9.5 ML) and thick (11 ML) Mn spacer layers, but firstly we expect such differences to be relatively small, and secondly they do not play a role when changing between parallel and antiparallel alignment of the Co magnetization directions at fixed Mn thickness. The capping Ni layer could have an influence on the dynamics as well, but it should influence all three cases equally and we expect it to behave identically to the top Co layer, as the R-XMCD hysteresis loop (Fig. S5 within the Supplemental Material [31]) indicates.

V. CONCLUSIONS

In summary, we probed element- and time-resolved ultrafast magnetization dynamics of two FM layers, magnetically coupled through an AFM spacer layer. From our measurements it is clear that the antiferromagnetic spacer layer and its spin structure have a significant effect on the magnetization dynamics of the FM layers after an optical pump. We show that the experimental results can be qualitatively reproduced by TD-DFT calculations and attribute their origin to the OISTR effect, where spin-selective optical excitation of electrons from occupied Co states into unoccupied Mn states act as an additional decay channel to enhance and accelerate demagnetization. Our findings provide further insight into the fundamental mechanisms that play a role in ultrafast magnetization dynamics. Accelerating demagnetization may be used in applications to improve dynamics for fast optical switching of magnetic order for spintronic devices or data storage.

ACKNOWLEDGMENTS

This work was supported by the Deutsche Forschungsgemeinschaft via the CRC/TRR 227 "Ultrafast Spin Dynamics", Project ID: 328545488, Projects A03, A04, and A07. We thank the Helmholtz-Zentrum Berlin für Materialien und Energie for the allocation of synchrotron radiation beamtime, and M. A. Mawass for assistance in using the FemtoSlicing Facility.

DATA AVAILABILITY

The data that support the findings of this article are openly available [40].

- E. Beaurepaire, J. C. Merle, A. Daunois, and J. Y. Bigot, Ultrafast spin dynamics in ferromagnetic nickel, Phys. Rev. Lett. 76, 4250 (1996).
- [2] J. Hohlfeld, E. Matthias, R. Knorren, and K. H. Bennemann, Nonequilibrium magnetization dynamics of nickel, Phys. Rev. Lett. 78, 4861 (1997).
- [3] A. Scholl, L. Baumgarten, R. Jacquemin, and W. Eberhardt, Ultrafast spin dynamics of ferromagnetic thin films observed by fs spin-resolved two-photon photoemission, Phys. Rev. Lett. **79**, 5146 (1997).
- [4] B. Koopmans, J. J. M. Ruigrok, F. Dalla Longa, and W. J. M. de Jonge, Unifying ultrafast magnetization dynamics, Phys. Rev. Lett. 95, 267207 (2005).
- [5] A. Kirilyuk, A. V. Kimel, and T. Rasing, Ultrafast optical manipulation of magnetic order, Rev. Mod. Phys. **82**, 2731 (2010).
- [6] J. Walowski and M. Münzenberg, Perspective: Ultrafast magnetism and THz spintronics, J. Appl. Phys. 120, 140901 (2016).
- [7] G. Malinowski, F. Dalla Longa, J. H. H. Rietjens, P. V. Paluskar, R. Huijink, H. J. M. Swagten, and B. Koopmans, Control of speed and efficiency of ultrafast demagnetization by direct transfer of spin angular momentum, Nat. Phys. 4, 855 (2008).
- [8] M. Battiato, K. Carva, and P. M. Oppeneer, Superdiffusive spin transport as a mechanism of ultrafast demagnetization, Phys. Rev. Lett. 105, 027203 (2010).
- [9] A. Melnikov, I. Razdolski, T. O. Wehling, E. T. Papaioannou, V. Roddatis, P. Fumagalli, O. Aktsipetrov, A. I. Lichtenstein, and U. Bovensiepen, Ultrafast transport of laser-excited spinpolarized carriers in Au/Fe/MgO(001), Phys. Rev. Lett. 107, 076601 (2011).
- [10] D. Rudolf, C. La-O-Vorakiat, M. Battiato, R. Adam, J. M. Shaw, E. Turgut, P. Maldonado, S. Mathias, P. Grychtol, H. T. Nembach *et al.*, Ultrafast magnetization enhancement in metallic multilayers driven by superdiffusive spin current, Nat. Commun. 3, 1037 (2012).

- [11] A. Eschenlohr, M. Battiato, P. Maldonado, N. Pontius, T. Kachel, K. Holldack, R. Mitzner, A. Föhlisch, P. M. Oppeneer, and C. Stamm, Ultrafast spin transport as key to femtosecond demagnetization, Nat. Mater. 12, 332 (2013).
- [12] I. Kumberg, E. Golias, N. Pontius, R. Hosseinifar, K. Frischmuth, I. Gelen, T. Shinwari, S. Thakur, C. Schüßler-Langeheine, P. M. Oppeneer, and W. Kuch, Accelerating the laser-induced demagnetization of a ferromagnetic film by antiferromagnetic order in an adjacent layer, Phys. Rev. B 102, 214418 (2020).
- [13] E. Carpene, E. Mancini, C. Dallera, M. Brenna, E. Puppin, and S. de Silvestri, Dynamics of electron-magnon interaction and ultrafast demagnetization in thin iron films, Phys. Rev. B 78, 174422 (2008).
- [14] E. Iacocca, T.-M. Liu, A. H. Reid, Z. Fu, S. Ruta, P. W. Granitzka, E. Jal, S. Bonetti, A. X. Gray, C. E. Graves *et al.*, Spin-current-mediated rapid magnon localisation and coalescence after ultrafast optical pumping of ferrimagnetic alloys, Nat. Commun. 10, 1756 (2019).
- [15] C. Stamm, T. Kachel, N. Pontius, R. Mitzner, T. Quast, K. Holldack, S. Khan, C. Lupulescu, E. F. Aziz, M. Wietstruk et al., Femtosecond modification of electron localization and transfer of angular momentum in nickel, Nat. Mater. 6, 740 (2007).
- [16] B. Koopmans, G. Malinowski, F. Dalla Longa, D. Steiauf, M. Fähnle, T. Roth, M. Cinchetti, and M. Aeschlimann, Explaining the paradoxical diversity of ultrafast laser-induced demagnetization, Nat. Mater. 9, 259 (2010).
- [17] M. Sultan, U. Atxitia, A. Melnikov, O. Chubykalo-Fesenko, and U. Bovensiepen, Electron- and phonon-mediated ultrafast magnetization dynamics of Gd(0001), Phys. Rev. B 85, 184407 (2012).
- [18] J. K. Dewhurst, P. Elliott, S. Shallcross, E. K. U. Gross, and S. Sharma, Laser-induced intersite spin transfer, Nano Lett. 18, 1842 (2018).

- [19] F. Siegrist, J. A. Gessner, M. Ossiander, C. Denker, Y.-P. Chang, M. C. Schröder, A. Guggenmos, Y. Cui, J. Walowski, U. Martens *et al.*, Light-wave dynamic control of magnetism, Nature (London) 571, 240 (2019).
- [20] F. Willems, C. von Korff Schmising, C. Strüber, D. Schick, D. W. Engel, J. K. Dewhurst, P. Elliott, S. Sharma, and S. Eisebitt, Optical inter-site spin transfer probed by energy and spin-resolved transient absorption spectroscopy, Nat. Commun. 11, 871 (2020).
- [21] E. Golias, I. Kumberg, I. Gelen, S. Thakur, J. Gördes, R. Hosseinifar, Q. Guillet, J. K. Dewhurst, S. Sharma, C. Schüßler-Langeheine, N. Pontius, and W. Kuch, Ultrafast optically induced ferromagnetic state in an elemental antiferromagnet, Phys. Rev. Lett. 126, 107202 (2021).
- [22] S. A. Ryan, P. C. Johnsen, M. F. Elhanoty, A. Grafov, N. Li, A. Delin, A. Markou, E. Lesne, C. Felser, O. Eriksson *et al.*, Optically controlling the competition between spin flips and intersite spin transfer in a Heusler half-metal on sub-100-fs time scales, Sci. Adv. 9, eadi1428 (2023).
- [23] C. Möller, H. Probst, G. S. M. Jansen, M. Schumacher, M. Brede, J. K. Dewhurst, M. Reutzel, D. Steil, S. Sharma, and S. Mathias, Verification of ultrafast spin transfer effects in ironnickel alloys, Commun. Phys. 7, 74 (2024).
- [24] K. Bobowski, X. Zheng, B. Frietsch, D. Lawrenz, W. Bronsch, C. Gahl, B. Andres, C. Strüber, R. Carley, M. Teichmann *et al.*, Ultrafast spin transfer and its impact on the electronic structure, Sci. Adv. 10, eadn4613 (2024).
- [25] B. Zhang, C.-B. Wu, and W. Kuch, Tailoring interlayer coupling and coercivity in Co/Mn/Co trilayers by controlling the interface roughness, J. Appl. Phys. 115, 233915 (2014).
- [26] Y. A. Shokr, M. Erkovan, C.-B. Wu, B. Zhang, O. Sandig, and W. Kuch, Temperature-induced sign change of the magnetic interlayer coupling in Ni/Ni₂₅ Mn₇₅/Ni trilayers on Cu₃ Au(001), J. Appl. Phys. 117, 175302 (2015).
- [27] L. Néel, Sur un nouveau mode de couplage entre les aimantations de deux couches minces ferromagnétiques, C. R. Hebd. Seances Acad. Sci. 255, 1676 (1962).
- [28] B. Dieny, V. S. Speriosu, S. S. P. Parkin, B. A. Gurney, D. R. Wilhoit, and D. Mauri, Giant magnetoresistance in soft ferromagnetic multilayers, Phys. Rev. B 43, 1297 (1991).
- [29] K. Holldack, J. Bahrdt, A. Balzer, U. Bovensiepen, M. Brzhezinskaya, A. Erko, A. Eschenlohr, R. Follath, A. Firsov, W. Frentrup *et al.*, FemtoSpeX: A versatile optical pump-soft x-ray probe facility with 100 fs x-ray pulses of variable polarization, J. Synchrotron Radiat. 21, 1090 (2014).
- [30] I. Kumberg, E. Golias, S. E. Hadjadj, R. Hosseinifar, S. Thakur, T. Shinwari, I. Gelen, N. Pontius, C. Schüßler-Langeheine, C. von Korff Schmising, S. Sharma, and W. Kuch, Ultrafast laserinduced magneto-optical changes in resonant magnetic x-ray reflectivity, Phys. Rev. B 108, 054439 (2023).
- [31] See Supplemental Material at http://link.aps.org/supplemental/ 10.1103/h2cw-hdvm for additional details and referencing Refs. [41–47].

- [32] K. Ohta and H. Ishida, Matrix formalism for calculation of electric field intensity of light in stratified multilayered films, Appl. Opt. 29, 1952 (1990).
- [33] K. Ohta and H. Ishida, Matrix formalism for calculation of the light beam intensity in stratified multilayered films, and its use in the analysis of emission spectra, Appl. Opt. 29, 2466 (1990).
- [34] T. Roth, A. J. Schellekens, S. Alebrand, O. Schmitt, D. Steil, B. Koopmans, M. Cinchetti, and M. Aeschlimann, Temperature dependence of laser-induced demagnetization in Ni: A key for identifying the underlying mechanism, Phys. Rev. X 2, 021006 (2012).
- [35] J. K. Dewhurst, K. Krieger, S. Sharma, and E. Gross, An efficient algorithm for time propagation as applied to linearized augmented plane wave method, Comput. Phys. Commun. 209, 92 (2016).
- [36] http://elk.sourceforge.net.
- [37] P. Elliott, T. Müller, J. K. Dewhurst, S. Sharma, and E. K. U. Gross, Ultrafast laser induced local magnetization dynamics in Heusler compounds, Sci. Rep. 6, 38911 (2016).
- [38] J. K. Dewhurst, S. Shallcross, E. K. U. Gross, and S. Sharma, Substrate-controlled ultrafast spin injection and demagnetization, Phys. Rev. Appl. **10**, 044065 (2018).
- [39] M. Battiato, K. Carva, and P. M. Oppeneer, Theory of laser-induced ultrafast superdiffusive spin transport in layered heterostructures, Phys. Rev. B 86, 024404 (2012).
- [40] J. Gördes, I. Kumberg, A. S. Chowdhury, M. Walter, T. Shinwari, S. Thakur, S. Sharma, C. Schüßler-Langeheine, N. Pontius, and W. Kuch, Accelerated ultrafast demagnetization of an interlayer-exchange-coupled Co/Mn/Co trilayer [Data set]. Zenodo (2025), https://doi.org/10.5281/zenodo.15552577.
- [41] S. Macke and E. Goering, Magnetic reflectometry of heterostructures, J. Phys.: Condens. Matter 26, 363201 (2014).
- [42] https://www.remagx.org/.
- [43] B. L. Henke, E. M. Gullikson, and J. C. Davis, X-ray interactions: Photoabsorption, scattering, transmission, and reflection at $E = 50 30,000 \,\text{eV}$, Z = 1 92, At. Data Nucl. Data Tables **54**, 181 (1993).
- [44] M. Abu-Joudeh, B. Davies, and P. Montano, LEED, auger, and electron energy loss studies of Ni epitaxially grown on Cu(100), Surf. Sci. 171, 331 (1986).
- [45] J. R. Cerda, P. L. de Andres, A. Cebollada, R. Miranda, E. Navas, P. Schuster, C. M. Schneider, and J. Kirschner, Epitaxial growth of cobalt films on Cu(100): A crystallographic LEED determination, J. Phys.: Condens. Matter 5, 2055 (1993).
- [46] Q. Wang, N. Metoki, C. Morawe, T. Zeidler, and H. Zabel, Structural and magnetic properties of Co/face-centered-cubic Mn(001) multilayers, J. Appl. Phys. 78, 1689 (1995).
- [47] P. Johnson and R. Christy, Optical constants of transition metals: Ti, V, Cr, Mn, Fe, Co, Ni, and Pd, Phys. Rev. B 9, 5056 (1974).